

See discussions, stats, and author profiles for this publication at: <http://www.researchgate.net/publication/252458732>

# Medium resolution imaging spectrometer (MERIS) estimation of chlorophyll-a concentration in the turbid sediment-laden waters of the Changjiang (Yangtze) Estuary

ARTICLE *in* INTERNATIONAL JOURNAL OF REMOTE SENSING · SEPTEMBER 2010

Impact Factor: 1.65 · DOI: 10.1080/01431161.2010.485216

---

CITATIONS

11

READS

69

5 AUTHORS, INCLUDING:



Fang Shen

East China Normal University

121 PUBLICATIONS 383 CITATIONS

[SEE PROFILE](#)



Mhd Suhyb Salama

University of Twente

50 PUBLICATIONS 399 CITATIONS

[SEE PROFILE](#)

## Medium resolution imaging spectrometer (MERIS) estimation of chlorophyll-*a* concentration in the turbid sediment-laden waters of the Changjiang (Yangtze) Estuary

FANG SHEN\*†, YUN-XUAN ZHOU†, DAO-JI LI†, WEI-JIAN ZHU†  
and MHD SUHYB SALAMA‡

†State Key Laboratory of Estuarine and Coastal Research, East China Normal University, Shanghai 200062, China

‡International Institute for Geo-information Science and Earth Observation, Enschede 7500AA, The Netherlands

Satellite estimation of chlorophyll-*a* (Chl-*a*) concentration in the Changjiang Estuary is challenging for ocean-colour retrieval algorithms. The Changjiang Estuary is characterized by suspended-sediment-dominated waters in the mouth and optically complex case 2 waters offshore of the mouth. Satellite ocean-colour products show that high-sediment loads of estuarine waters can cause overestimations or invalid flags of Chl-*a* concentration. A synthetic chlorophyll index (SCI) was designed for extracting chlorophyll information and for minimizing the influence of sediments on the remote-sensing reflectance spectrum. An SCI algorithm, a quadratic polynomial function of the SCI versus Chl-*a* concentration, was applied to the estimation of Chl-*a* concentration from Medium Resolution Imaging Spectrometer (MERIS) images. The overestimation of Chl-*a* concentration was corrected. The SCI algorithm has applications for MERIS estimation of Chl-*a* concentration in turbid waters with a moderate to high suspended-sediment concentration.

### 1. Introduction

Remote sensing is an effective and convenient technique for synoptic monitoring of the health of coastal and marine ecosystems. Chlorophyll-*a* (Chl-*a*) concentration and primary production in oceanic waters (i.e. case 1 waters) can be estimated using satellite data from ocean-colour sensors (e.g. the Sea-viewing Wide Field-of-view Sensor (SeaWiFS), the Moderate Resolution Imaging Spectroradiometer (MODIS) and the Medium Resolution Imaging Spectrometer (MERIS)) (IOCCG 2006, Dasgupta *et al.* 2009). However, satellite estimation of Chl-*a* concentration is still difficult for coastal waters, where there are optically complex constituents consisting primarily of suspended-sediment matter, coloured dissolved organic matter (CDOM) and phytoplankton (i.e. case 2 waters) (IOCCG 2000). Although the current generation of satellite ocean-colour sensors has a number of wavebands in the visible spectral range, for case 2 water constituents and concentrations, it is still difficult to develop retrieval algorithms using remote-sensing signals because the water constituents vary independently.

Remote-sensing reflectance in the blue and green parts of the spectral range, as used for developing SeaWiFS and MODIS algorithms of Chl-*a* estimates for case 1 waters (O'Reilly *et al.* 1998), can affect estimates for case 2 waters because of CDOM and tripton absorptions (IOCCG 2000, Cannizzaro and Carder 2006). Thus, when applied

\*Corresponding author. Email: fshen@sklec.ecnu.edu.cn

to case 2 waters, the algorithm of blue-to-green ratios of remote-sensing reflectance can produce large biases in the Chl-*a* estimate. Recent efforts have modified existing, or developed new, algorithms for case 2 waters. The bio-optical GSM01 algorithm, implemented in the SeaDAS software package, was modified for MODIS Chl-*a* estimation of Canadian case 2 waters (Komick *et al.* 2009) and the Dutch Lakes (Salama *et al.* 2009). The blue-to-green reflectance ratio being shifted to the near-infrared (NIR) to red reflectance ratio using SeaWiFS and MODIS data (Dall'Olmo and Gitelson 2005, 2006, Gitelson *et al.* 2007) and MERIS data (Gons *et al.* 2008) was proposed for Chl-*a* estimates of turbid productive waters. The MERIS case 2 waters processor (C2P) (Doerffer and Schiller 2008), a plug-in module of Beam VISAT 4.5 (<http://www.brockmann-consult.de/beam>), was designed for case 2 waters application based on a neural-network inversion scheme for MERIS Chl-*a* estimation (Doerffer and Schiller 2007).

The Changjiang Estuary presents challenges for satellite Chl-*a* estimation because of its high suspended-sediment concentrations (SSCs). Morel and Bélanger (2006) designated it as case 2S water, i.e. sediment-laden turbid waters (rather than yellow-substance-dominated water). Remote-sensing reflectance is enhanced in case 2S waters because of increased scattering (rather than absorption), which affects the whole spectral range (Morel and Bélanger 2006). The increased reflectance can mask the spectral features of chlorophyll causing errors in the Chl-*a* estimate. Woźniak and Stramski (2004) reported that using the algorithm of blue-to-green ratios of remote-sensing reflectance can produce Chl-*a* overestimates from 50% to 2000%, when the SSC is  $1 \text{ mg l}^{-1}$  and the Chl-*a* is  $0.05 \text{ mg m}^{-3}$ . Likewise, in the Changjiang Estuary, the results shown in §3.5 indicate that the MERIS-derived Chl-*a* with the C2P would be overestimated when the SSC is above  $50 \text{ mg l}^{-1}$ , as compared with the *in situ* Chl-*a*.

The objective of this study is to improve the accuracy of MERIS Chl-*a* estimates of sediment-laden water. Because of the invalid flag or overestimation of Chl-*a* for turbid waters that results from application of SeaWiFS, MODIS or MERIS standard ocean-colour algorithms, a new method is required for Chl-*a* estimates from satellite data in the presence of moderate or high SSCs. This will improve understanding of satellite monitoring of estuarine and coastal ecosystem variability and warnings of algal blooms.

## 2. Data collection and methods

### 2.1 Study area

The Changjiang River drainage area is about  $1.8 \times 10^6 \text{ km}^2$ , which includes several metropolises (e.g. Chongqing, Wuhan and Shanghai), and it has a mainly agricultural economy. A large amount of material is carried by the river into the Changjiang Estuary and the East China Sea. Shen (1991) reported the annual river flux and sediment loads at  $9.03 \times 10^{11} \text{ m}^3$  and  $4.14 \times 10^8 \text{ tonnes}$ , respectively and the annual fluxes of dissolved inorganic nitrogen (DIN), phosphorus ( $\text{PO}_4\text{-P}$ ) and silicon ( $\text{SiO}_3\text{-Si}$ ) were  $7.84 \times 10^5$ ,  $1.51 \times 10^4$  and  $2.22 \times 10^6 \text{ tonnes}$ , respectively. During a single large flood in 1998, the total nitrogen (TN) and DIN fluxes reached  $2.85 \times 10^6$  and  $1.75 \times 10^6 \text{ tonnes}$ , respectively (Shen 2004). With rapid developments in the economy and the strong effects of anthropogenic activity in the drainage area, nutrient loadings into the Changjiang Estuary have increased dramatically in the last two decades because of increased sewage discharge, overuse of agriculture fertilizers and industrial effluents (Gao and Song 2005). Consequently, algal blooms are common in the Changjiang Estuary and the adjacent East China Sea (e.g. a range of  $30^\circ 30' - 32^\circ 00'$  N latitude and  $122^\circ 15' - 123^\circ 15'$  E longitude). Serious eutrophication

caused by high nutrient loadings in the area has led to a change in the species composition, food-chain structure and element cycling in the marine ecosystem (Gao and Song 2005).

The Changjiang Estuary is characterized by highly turbid waters; it has complex hydrodynamics and seasonal discharges of sediment. The SSC ranges from  $20 \text{ mg l}^{-1}$  (i.e. offshore of the mouth) to  $2500 \text{ mg l}^{-1}$  or more (e.g. in the turbidity maximum zone; Li *et al.* 1994). In the mouth of the estuary (i.e.  $122^{\circ} 15' \text{ E}$  longitude riverwards), the mean SSC range is  $100\text{--}300 \text{ mg l}^{-1}$  (He *et al.* 1999, Kong *et al.* 2006), and the water is typically turbid sediment-dominated case 2 waters. Offshore of the mouth (i.e. from the turbidity front to the riverine plume front seawards), the SSC sharply decreases to less than  $100 \text{ mg l}^{-1}$ , with a mean value of  $20\text{--}50 \text{ mg l}^{-1}$ , and the water is typically optically complex case 2 waters with various constituents including phytoplankton, CDOM and mineral particles.

The turbidity front dividing line moves riverwards and seawards with the alternation of the spring-neap tidal cycle and flood-ebb tide. Optically, the waters have a clear distinction, i.e. the sediment-dominated case 2 water in the ‘A’ zone and the multicomponent case 2 water in the ‘B’ zone (see figure 1).

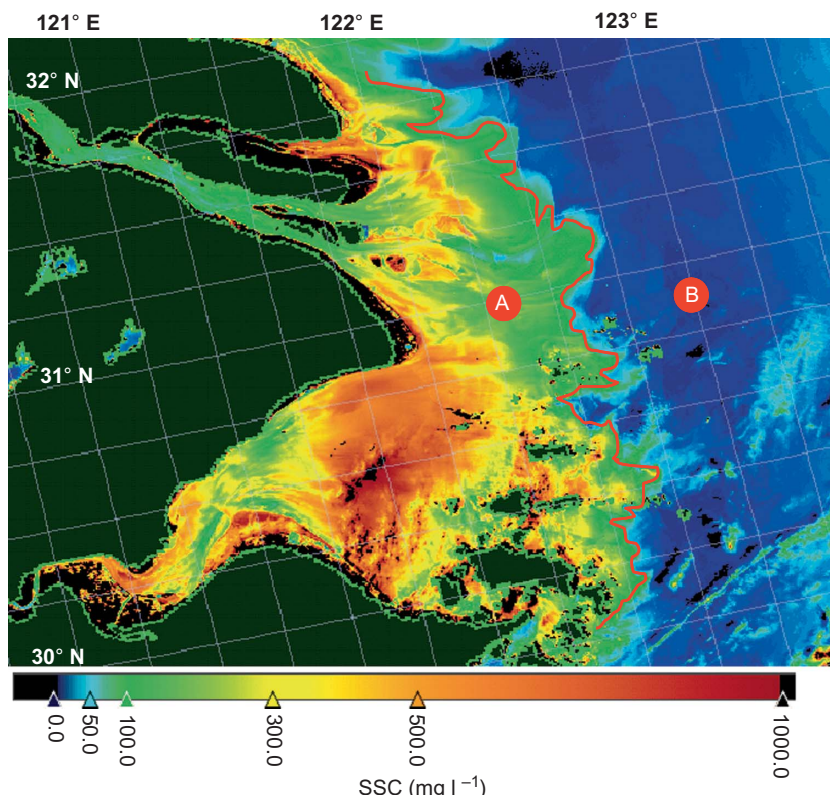


Figure 1. Sketch map of optically separated waters in the Changjiang Estuary. The turbidity front dividing line (red line) optically separates the waters into the sediment-dominated waters ('A' zone) and the multicomponent case 2 water ('B' zone). The SSC image is derived from MERIS full-resolution data on 25 April 2008 using an algorithm described in Shen *et al.* (in press).

## 2.2 In situ datasets

*In situ* datasets were collected on cruises in the Changjiang Estuary and the adjacent coastal sea during the early spring and summer seasons of 2008. The early spring cruise from 22 April to 1 May comprised 57 stations from 29.5°–32.0° N latitude and 121.5°–124.0° E longitude (see figure 2(a)). The summer cruise from 3 to 6 August comprised 31 stations from 30.9°–31.4° N latitude and 121.5°–123.1° E longitude (see figure 2(b)). *In situ* Chl-*a* for the early spring dataset was generally lower (i.e.  $\sim < 3$  mg m<sup>-3</sup>) than that for the summer dataset, possibly because of the limited riverine discharges in the dry season and low temperatures in the early spring. *In situ*, above-water radiometric measurements were limited to when weather conditions (e.g. wind speed and sunlight) were suitable, and were conducted concurrently with sampling of the water surface at 20 stations during the spring cruise and at 23 stations during the summer cruise. *In situ* SSC and Chl-*a* were determined in the laboratory by analyses of simultaneously collected water samples.

## 2.3 Remote-sensing reflectance from radiometric measurements

Remote-sensing reflectance ( $R_{rs}$ ) was defined as  $R_{rs} = \frac{L_w(\lambda)}{E_d(0^+)}$  (Carder *et al.* 1993, Mobley 1999), where  $E_d(0^+)$  is the downwelling irradiance just above the sea surface and  $L_w(\lambda)$  is the directional water-leaving radiance. Both of these were obtained from the above-surface radiometric measurements according to the NASA protocol of optical measurements (NASA 2003), using the ASD Field spectroradiometer (<http://www.asdi.com>). The approach for the measurements can be seen in further detail in Lee *et al.* (1996) and Mobley (1999).

## 2.4 Laboratory analysis

At all stations, chlorophyll concentrations were determined using the fluorometric method. *In situ* water samples were immediately filtered through 0.7 µm Whatman GF/F glass-fibre filters. The filters with the material retained were stored in liquid nitrogen and then transferred to the laboratory for Chl-*a* concentration analysis. A Hitachi F-2500 fluorescence spectrophotometer was used for measuring and calculating Chl-*a* concentration in the laboratory according to the JGOFS standard protocol

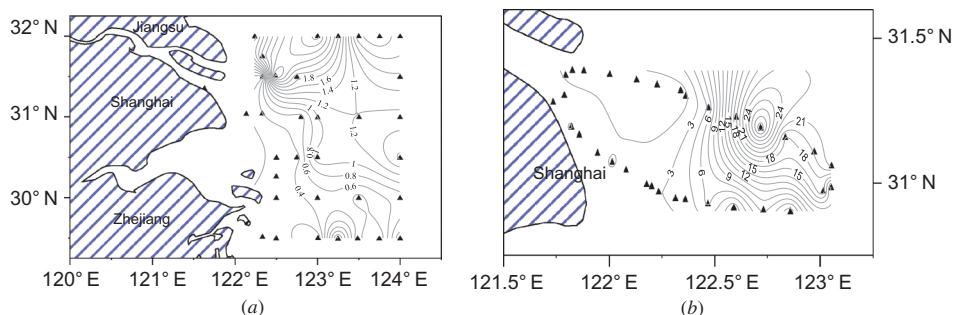


Figure 2. Isoline maps of the spatial distribution of ship-derived chlorophyll-*a* concentrations (Chl-*a*) in the Changjiang Estuary. The Chl-*a* data were collected during (a) spring (22 April–1 May 2008) and (b) summer (3–6 August 2008) cruises. The solid triangle symbols denote *in situ* stations.

for measurement of chlorophyll (JGOFS 1998) and the Ocean Optics Protocols for Satellite Ocean Colour Sensor Validation (Trees *et al.* 2003).

The magnitude of the SSC was determined gravimetrically in the laboratory by filtering the water sample on a 0.7 µm Whatman GF/F glass-fibre filter pre-weighted. The filter was rinsed with Milli-Q water to remove salts, dried and then reweighed on a high-precision balance.

## 2.5 MERIS data

MERIS data have deliverable level 1b and level 2 products for users after processing via the ground service segments. MERIS level 1b products include radiances at top-of-atmosphere (TOA). MERIS level 2 products include atmospherically corrected normalized surface reflectance and ocean-colour products, including total\_susp (total suspended matter dry weight concentration) and algal\_2 (Chl-a concentration over case 2 waters). However, the MERIS level 2 images of algal\_2 and normalized surface reflectance at all wavebands for the highly turbid estuary (around 122.6° E longitude riverwards) were flagged as ‘invalid’. As an extension of the regional case 2 waters products, the C2P on MERIS level 1b TOA radiances can produce new non-flagged water-leaving radiance reflectance and ocean-colour products for the estuary.

MERIS level 1b images covering the study area for 2008, with full and reduced resolution (FR and RR), were collected. During the two ship campaigns, coincident cloud-free images of MERIS overpasses on 25 April and 5 August were available.

## 2.6 Algorithm development

The MERIS NIR to red reflectance ratio can be correlated with Chl-a for turbid productive waters (i.e. Chl-a > 4 mg m<sup>-3</sup>) (Gons *et al.* 2008). However, for case 2S waters, the ratio algorithm would introduce errors to the Chl-a estimation that are probably caused by sediment scattering in the NIR part of the spectral range when the SSC level is high. Fluorescence line height (FLH) is an index that is better associated with Chl-a in coastal waters (Gower and Borstad 2004). However, the FLH is poorly related to the Chl-a in our case (see figures 5(a) and 5(b)). Therefore, developing a new algorithm of extracting Chl-a for this case is an urgent need. The new algorithm is based on MERIS water-leaving radiance reflectance (i.e. remote-sensing reflectance) products by the C2P.

A synthetic chlorophyll index (SCI) was developed for extracting chlorophyll information and minimizing the sediment influence from the remote-sensing reflectance spectrum. The SCI takes the variability of spectral reflectance features of chlorophyll and sediment into account synthetically. We introduced two parameters,  $H_{\text{chl}}$  and  $H_{\Delta}$ , for the SCI. The  $H_{\text{chl}}$  was used a proxy for the chlorophyll pigments, and it was calculated by the following formula:

$$H_{\text{chl}} = \left[ R_{\text{rs}}(\lambda_4) + \frac{\lambda_4 - \lambda_3}{\lambda_4 - \lambda_2} (R_{\text{rs}}(\lambda_2) - R_{\text{rs}}(\lambda_4)) \right] - R_{\text{rs}}(\lambda_3). \quad (1)$$

If the wavelengths,  $\lambda_2$ ,  $\lambda_3$  and  $\lambda_4$ , are given MERIS bands 620, 665 and 681 nm, respectively, the formula can be simplified with the weighted sum to:

$$\begin{aligned} H_{\text{chl}} &= (0.74R_{\text{rs}}(681) + 0.26R_{\text{rs}}(620)) - R_{\text{rs}}(665), \\ H_{\text{chl}} &< 0, \text{ if and only if } R_{\text{rs}}(665) > 0.74R_{\text{rs}}(681) + 0.26R_{\text{rs}}(620). \end{aligned} \quad (2)$$

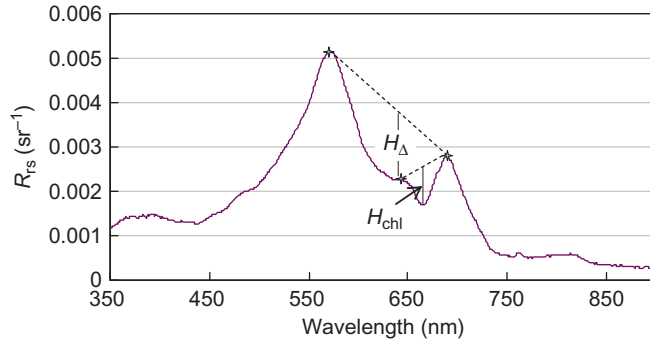


Figure 3. Sketch map of the synthetic chlorophyll index (SCI) designed by modelling of remote-sensing reflectance ( $R_{rs}$ ) and chlorophyll-*a* concentration (Chl-*a*).  $H_{chl}$  is a measure of the distinct absorption dip of the reflectance spectrum at the MERIS band 665 nm below (positive) and above (negative) the baseline connecting the  $R_{rs}$  at MERIS bands 620 and 681 nm (620 and 681 nm are reference wavebands).  $H_\Delta$  is the relative height of  $R_{rs}$  at 620 nm below (negative) and above (positive) the baseline (two reference wavebands: 560 and 681 nm).

Equation (2) defines  $H_{chl}$  as a measure of the distinct absorption dip of the reflectance spectrum at the MERIS band 665 nm below (positive) and above (negative) the baseline connecting  $R_{rs}$  at MERIS bands 620 nm and 681 nm (the two bands 620 and 681 nm are reference bands) (see figure 3). By avoiding maximum absorption of the CDOM in the blue part of the spectral range and assuming that the CDOM absorption at wavelengths larger than 555 nm is negligible,  $R_{rs}$  at 620, 665 and 681 nm is affected by phytoplankton in the absence of sediment.  $R_{rs}$  at 665 nm is minimal due to maximum absorption by chlorophyll pigments. In this case,  $R_{rs}$  at 665 nm is generally below the baseline, leading to positive  $H_{chl}$  (+). A negative  $H_{chl}$  (-) can be interpreted as a lack of chlorophyll pigments, or the presence of high SSCs.

Another parameter,  $H_\Delta$ , is introduced into the function of the SCI as a correction factor for  $H_{chl}$  in the presence of mid- or high-sediment loads.  $H_\Delta$  was using:

$$H_\Delta = R_{rs}(\lambda_2) - \left[ R_{rs}(\lambda_4) + \frac{\lambda_4 - \lambda_2}{\lambda_4 - \lambda_1} (R_{rs}(\lambda_1) - R_{rs}(\lambda_4)) \right]. \quad (3)$$

If the wavelengths,  $\lambda_1$ ,  $\lambda_2$  and  $\lambda_4$ , are given MERIS bands 560, 620 and 681 nm, respectively, the formula can be simplified with a weighted sum to:

$$\begin{aligned} H_\Delta &= R_{rs}(620) - 0.5(R_{rs}(560) + R_{rs}(681)), \\ H_\Delta &< 0 \text{ if and only if } R_{rs}(620) < 0.5R_{rs}(560) + 0.5R_{rs}(681). \end{aligned} \quad (4)$$

$H_\Delta$  is the relative height of  $R_{rs}$  at 620 nm below (negative) and above (positive) the baseline (two reference wavebands: 560 and 681 nm) (see figure 3). By assuming that absorptions of water constituents at 560, 620 and 681 nm are minimal,  $H_\Delta$  fluctuation is attributed to the effects of scattering by the total particulates.

The study in Shen *et al.* (in press) indicated that the sensitivity of  $R_{rs}$  to the SSC can be displaced from a shorter to a longer wavelength with increasing SSC.  $R_{rs}$  at the MERIS band 620 nm is more sensitive to the moderate SSC ranging from 20 to 80 mg l<sup>-1</sup> than at other bands. In this range of SSC, the  $R_{rs}$  spectrum is modulated by equivalent spectral features of both the sediment and chlorophyll, leading to a larger bias in the Chl-*a* estimation that is caused by mixed  $R_{rs}$  spectral signatures. The  $R_{rs}$  spectrum is

dominated by the spectral characteristics of the chlorophyll pigments in the case of low SSC levels (e.g.  $< 20 \text{ mg l}^{-1}$ ) and by the characteristics of the sediment in the case of high SSC levels (e.g.  $> 100 \text{ mg l}^{-1}$ ). We inferred that Chl-*a* estimation from mixed or sediment-dominant  $R_{rs}$  spectra would introduce larger errors because of interference of the spectral signatures of sediment in the presence of moderate or high SSC, if the effects of  $H_\Delta$  on the Chl-*a* estimation were not considered.

Therefore, the SCI, a synthetic index that links the  $H_{chl}$  and  $H_\Delta$  parameters, was defined simply as:

$$\text{SCI} = H_{chl} - H_\Delta. \quad (5)$$

The SCI is a function of the difference of both variables. The SCI should be a significant function of Chl-*a*, if the functions of  $H_{chl}$  versus Chl-*a* and  $H_\Delta$  versus Chl-*a* exist.

It seems likely that  $H_{chl}$  could have a strong relationship with Chl-*a*. Thus, the SCI was interpreted as a corrected  $H_{chl}$  to suppress the influence of the sediment. For instance, assuming Chl-*a* is fixed,  $H_{chl}$ , being the relative height (distance from  $R_{rs}$  at 665 nm to the baseline connecting  $R_{rs}$  at 620 and 681 nm), will increase if  $R_{rs}$  at 620 nm increases with increasing SSC. Thus, if only the function of  $H_{chl}$  versus Chl-*a* is used to estimate Chl-*a*, the increase in  $H_{chl}$  would lead to Chl-*a* overestimation of turbid water. Corresponding to the increase in  $H_{chl}$ ,  $H_\Delta$  will also increase because of an increase in  $R_{rs}$  at 620 nm. Thus, the subtraction of  $H_\Delta$  from  $H_{chl}$  balances out the effect due to the increased SSC, thereby ensuring that the output from SCI is unaffected by the increased  $R_{rs}$  at 620 nm due to scattering by suspended particles.

For the presence of blue-green algae in waters,  $R_{rs}$  at 620 nm will decrease because of the effect of absorption by phycocyanin; the  $H_{chl}$  (+) value will reduce and the absolute value of  $H_\Delta$  (-) will increase. Therefore, negative  $H_\Delta$  (-) becomes a compensating factor for the decrease in  $H_{chl}$  (+) in the calculation of SCI, and the SCI value also does not change in this case.

### 3. Results

#### 3.1 In situ SSC and Chl-*a*

Statistical parameters for the *in situ* data are listed in table 1. The *in situ* Chl-*a* showed seasonal and spatial variation. Figure 2(a) showed that the *in situ* Chl-*a* values ranged from 0.03 to  $3.10 \text{ mg m}^{-3}$  for the 34 stations from the early spring cruise. Out of these stations, 58.8% had Chl-*a*  $< 1 \text{ mg m}^{-3}$ , and 41.2% had Chl-*a* ranging from 1 to  $3.1 \text{ mg m}^{-3}$ . In contrast, the Chl-*a* values ranged from 0.88 to  $31.5 \text{ mg m}^{-3}$  (mean value of  $6.76 \text{ mg m}^{-3}$ ) for the 29 stations from the summer cruise (figure 2(b)). Out of these stations, 75.9% had Chl-*a* ranging from 0.88 to  $10 \text{ mg m}^{-3}$ , and 24.1% had Chl-*a* above  $10 \text{ mg m}^{-3}$ . Spatially, *in situ* Chl-*a* was higher in the 'B' zone than in the 'A' zone. During summer, the observed Chl-*a* was an order of magnitude or more higher in the 'B' zone than in the 'A' zone (table 1). The results implied that temperature and turbidity played a role in the spatial distribution of Chl-*a*. Low temperature and high turbidity (e.g.  $\text{SSC} > 100 \text{ mg l}^{-1}$ ) in the mouth could limit algal growth; low Chl-*a* values (i.e. below  $1 \text{ mg m}^{-3}$ ) were observed during the early spring campaign. In contrast, high temperatures during the summer and relatively lower turbidity offshore of the mouth, could promote algal blooms; high Chl-*a* (i.e. above  $10 \text{ mg m}^{-3}$ ) was observed during the summer campaign.

Table 1. *In situ* datasets obtained from two cruises in the Changjiang Estuary during the early spring and the summer seasons of 2008. The ‘A’ zone is characterized by turbid sediment waters and the ‘B’ zone by optically complex case 2 waters. Statistical parameters such as the minimum, maximum, median, mean and standard deviation (SD) of the *in situ* data are listed.

Survey date	Location	Data	Minimum	Maximum	Median	Mean	SD
April 2008	‘A’ zone	Chl- <i>a</i> ( $\text{mg m}^{-3}$ )	0.06	2.50	0.27	0.57	0.86
		SSC ( $\text{mg l}^{-1}$ )	24.30	264.50	211.20	149.69	109.37
	‘B’ zone	Chl- <i>a</i> ( $\text{mg m}^{-3}$ )	0.03	3.10	0.84	1.02	0.81
		SSC ( $\text{mg l}^{-1}$ )	6.20	26.20	15.60	15.78	4.51
August 2008	‘A’ zone	Chl- <i>a</i> ( $\text{mg m}^{-3}$ )	0.88	6.31	1.66	2.09	1.38
		SSC ( $\text{mg l}^{-1}$ )	62.20	543.80	128.80	211.88	172.76
	‘B’ zone	Chl- <i>a</i> ( $\text{mg m}^{-3}$ )	4.69	31.50	17.75	16.31	9.08
		SSC ( $\text{mg l}^{-1}$ )	48.40	112.90	63.30	78.76	28.98

### 3.2 Patterns of remote-sensing reflectance spectra

The patterns of remote-sensing reflectance spectra measured from all stations during the two cruises showed large variability because of the diverse water constituents and variable concentrations. Figure 4 showed that the reflectance in the blue part of the spectral range basically tended to be low due to absorptions by CDOM and tripton. The fluctuations of the spectra were significant in the green and red parts in the presence of chlorophyll pigments. The reflectance peaks can shift from 490 or 510 nm for low Chl-*a* waters (see the spectra curves crossed by the dotted ellipse in figure 4(a)) to  $\sim$ 570 nm for moderate and high Chl-*a* waters (see the spectra curves crossed by the dashed ellipse in figures 4(a) and 4(b), and by the dashed-dotted ellipse in figure 4(b)). The  $R_{\text{rs}}$  spectra have a large trough at 670 nm (i.e. the peak of Chl-*a* absorption); the depth of the trough (i.e. the depth of Chl-*a* absorption) is significant for the manifestation of Chl-*a* (see the spectra curves crossed by the dashed-dotted ellipse in figure 4(b)).

The patterns showed sensitivity to SSC variation. Scattering caused by the sediment significantly influenced the amplitude of the reflectance spectrum in the whole visible and NIR spectral ranges (see the spectra curves crossed by the solid-line ellipse in

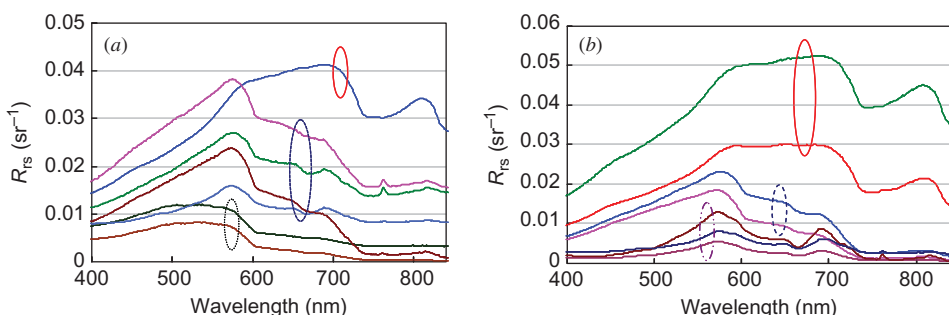


Figure 4. Examples of *in situ* remote-sensing reflectance spectra patterns from (a) the spring and (b) the summer datasets. The spectral curves crossed by the solid-line ellipses in (a) and (b) represent waters with high SSC (i.e.  $> 100 \text{ mg l}^{-1}$ ); the curves crossed by the dashed ellipse in both of (a) and (b) represent water with Chl-*a* below  $5 \text{ mg m}^{-3}$ ; the curves crossed by the dotted ellipse in (a) represent waters with low chlorophyll and sediment; the curves crossed by the dashed-dotted ellipse in (b) represent algal blooming waters with Chl-*a* above  $10 \text{ mg m}^{-3}$ .

figures 4(a) and 4(b)). The increased  $R_{rs}$  due to scattering by the sediment thus masked the fluctuations in the green and red parts. Therefore, it was difficult to identify chlorophyll in the sediment-laden waters. Overestimation in predicted chlorophyll concentrations can happen for samples with high SSCs (Gitelson *et al.* 2008).

### 3.3 SCI algorithm

Figures 5(a) and 5(b) show that the triangle points ( $H_{chl}$  versus *in situ* Chl-*a*) are linearly distributed.  $H_{chl}$  has a stronger linear regressive relationship with the *in situ* Chl-*a* at  $R^2 = 0.86$  (correlation coefficient square) and  $n = 23$  (the number of data samples), compared with that of FLH (employed wavebands: 665, 681 and 709 nm). Therefore, the function  $H_{chl}$  can be expressed as:

$$H_{chl} = \alpha_1 C_{chl} + \beta_1, \quad (6)$$

where  $C_{chl}$  stands for Chl-*a* and  $\alpha_1$  and  $\beta_1$  are fitting constants. The square points (FLH versus Chl-*a*) are dispersedly distributed. There is no applicable functional relationship for both in this case.

The relationship between  $H_\Delta$  and Chl-*a* was not predicted.  $H_\Delta$  could possibly be affected by both sediment and phytoplankton pigments. A negative logarithmic function fits the relationship between  $H_\Delta$  and Chl-*a*, and can be expressed as:

$$H_\Delta = -\alpha_2 \ln C_{chl} + \beta_2, \quad (7)$$

where the parameters  $\alpha_2$  and  $\beta_2$  are fitting constants. Figures 5(c) and 5(d) show the logarithmic regressions of  $H_\Delta$  and Chl-*a*, where the regressive Chl-*a* from equation (6), instead of *in situ* Chl-*a*, is employed to reduce uncertainty.

The negative logarithmic function seems reasonable. Because of the presence of lots of sediment particles in highly turbid waters, it is hard for incident sunlight to penetrate the water body, and phytoplankton grows slowly because of the lack of light energy; this causes a decrease in phytoplankton biomass relative to that in low-turbid waters.

Because  $H_{chl}$  and  $H_\Delta$  are both a function of Chl-*a*, we conclude that the SCI, a compounding index of both  $H_{chl}$  and  $H_\Delta$ , could also be a function of Chl-*a*. A quadratic polynomial function best fits the relationship between the SCI and Chl-*a*; this is:

$$SCI = \alpha_0 + \alpha_{11} C_{chl} + \alpha_{22} C_{chl}^2, \quad (8)$$

where the parameters  $\alpha_0$ ,  $\alpha_{11}$  and  $\alpha_{22}$  are fitting constants. Figures 5(e) and 5(f) show a quadratic polynomial regression between SCI and *in situ* Chl-*a*, respectively from the two datasets. It is evident in figures 5(e) or 5(f) that the SCI is better related to the Chl-*a*, with an improved correlation. As used for retrieval, the  $H_{chl}$  linear model,  $H_\Delta$  logarithmic model and SCI quadratic polynomial model are illustrated in figures 5(g) and 5(h) for the two corresponding datasets. Mathematical expressions of the SCI functions corresponding to the spring and summer datasets are listed in table 2.

### 3.4 Algorithm performance

The SCI algorithm for Chl-*a* estimation was performed for the MERIS images of water-leaving radiance reflectance, which was produced by the C2P. The resultant Chl-*a* derived from the MERIS FR image on 25 April 2008 and from the MERIS RR

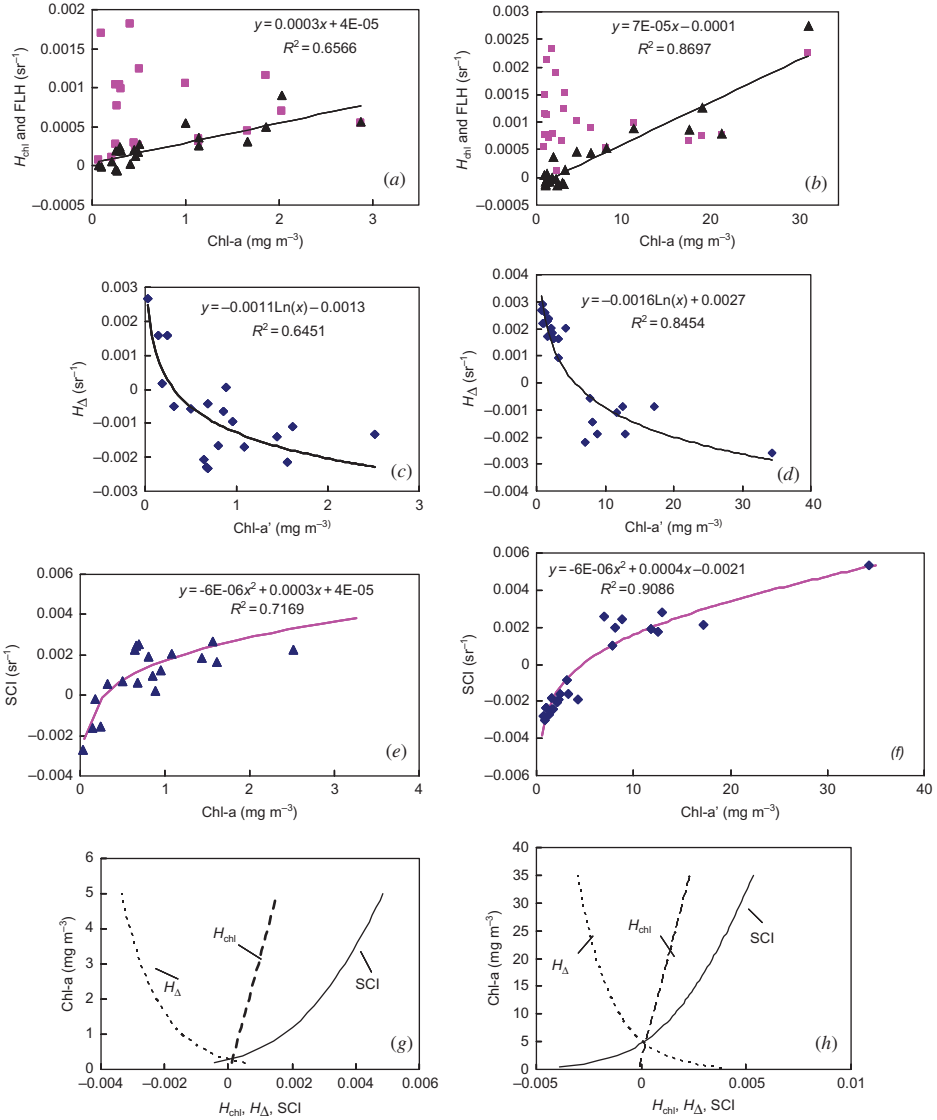


Figure 5. Modelling of  $H_{\text{chl}}$  versus Chl-a,  $H_{\Delta}$  versus Chl-a and SCI versus Chl-a. The linear regression of  $H_{\text{chl}}$  versus Chl-a is shown in (a) the spring and (b) the summer, where the triangle points denote  $H_{\text{chl}}$  versus Chl and the square points denote FLH versus Chl-a. The negative logarithmic regression of  $H_{\Delta}$  versus Chl-a is shown in (c) the spring and (d) the summer, where the regressive Chl-a (yield based on the linear model of  $H_{\text{chl}}$  versus Chl-a shown in (a) and (b)) was employed. The quadratic polynomial regression of SCI versus Chl-a is shown in (e) the spring and (f) the summer. The  $H_{\text{chl}}$  linear retrieval model,  $H_{\Delta}$  logarithmic retrieval model and SCI quadratic polynomial retrieval model are illustrated in (g) the spring dataset and (h) the summer dataset.

image on 5 August 2008 are shown in figure 6. The images correct for the overestimation of Chl-a in the mouth of the estuary, especially in the maximum turbidity zone, caused by the effect of sediment in the waters. The distribution of the derived Chl-a in the MERIS images formed a linguiform-like belt from north to south,

Table 2. Retrieval algorithms based on the SCI for estimation of chlorophyll-*a* concentrations for both the summer and spring datasets.

Datasets	Retrieval algorithms ( <i>y</i> : Chl- <i>a</i> in mg m <sup>-3</sup> ; <i>x</i> : SCI in sr <sup>-1</sup> )
From the spring	$y = 179378x^2 + 92.934x + 0.2736$
From the summer	$y = 550383x^2 + 2769x + 4.3866$

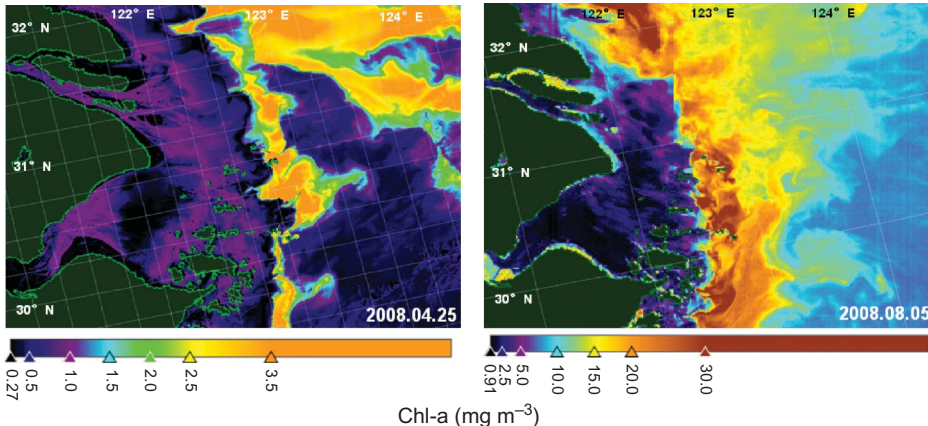


Figure 6. Chlorophyll-*a* concentration retrieved by the SCI algorithm from the MERIS FR image on 25 April and the RR image on 8 August 2008.

offshore of the mouth, which was similar to, though more detailed than that from, the *in situ* survey illustrated in figure 2 and similar to the results from *in situ* observations by Zhu (2004). The belt zone is situated seaward of the turbidity front, where SSC was lower (i.e. < 100 mg l<sup>-1</sup>) because of the deposition of a large amount of suspended sediment inside of the front riverwards. In addition, Chl-*a* would sometimes be high in the belt zone because nutrients carried by the river plume reaching the zone would cause phytoplankton to flourish, given sufficient light. Seaward of the zone, nutrient concentrations decline, and the water is more saline, leading to a decrease in phytoplankton biomass.

### 3.5 Comparison between *in situ* and MERIS-derived Chl-*a*

Figure 7 illustrates comparisons between *in situ* Chl-*a* and MERIS-SCI Chl-*a* (i.e. MERIS derived Chl-*a* by the SCI algorithm) and between *in situ* Chl-*a* and MERIS-C2P Chl-*a* (i.e. MERIS derived Chl-*a* by the C2P), for the spring and summer datasets respectively.

For the spring dataset, MERIS-SCI Chl-*a* versus *in situ* Chl-*a* (sampled on 24–30 April 2008 between 8:30 and 17:30 local time; the MERIS pass was at 10:07 on 25 April 2008) is shown in figure 7(a); for the summer dataset, MERIS-SCI Chl-*a* versus *in situ* data (sampled on 5 August 2008 between 8:30 and 17:30 local time; the MERIS pass was at 10:01 on the same day) is shown in figure 7(b). The root mean square errors (RMSEs) for the *in situ* Chl-*a* versus the MERIS-SCI Chl-*a* and MERIS-C2P Chl-*a* were calculated (see table 3). The Chl-*a* values improved when the SCI

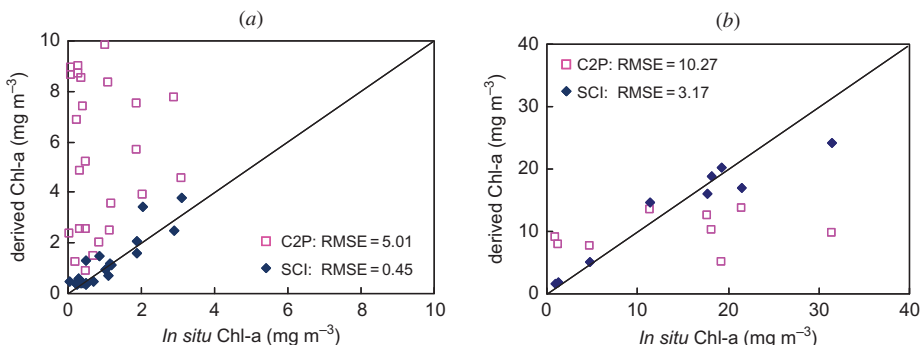


Figure 7. *In situ* Chl-*a* versus derived Chl-*a*. Filled squares denote *in situ* Chl-*a* versus MERIS-SCI Chl-*a* (MERIS derived Chl-*a* by the SCI algorithm). Open squares denote *in situ* Chl-*a* versus MERIS-C2P Chl-*a* (MERIS derived Chl-*a* by the C2P). The *in situ* dataset in (a) was sampled on 24–30 April 2008 between 8:30 and 17:30 local time (MERIS pass was at 10:07 on 25 April 2008) during the spring cruise. The *in situ* dataset in (b) was sampled on 5 August 2008 between 8:30 and 17:30 of local time (MERIS pass was at 10:01 on the same day) during the summer cruise.

Table 3. Root mean square errors (RMSEs) between *in situ* and MERIS-derived Chl-*a*. The derived Chl-*a* values were produced by the C2P and the SCI algorithm. The *in situ* datasets were from the spring and summer cruises.

Datasets	RMSE in Chl- <i>a</i> ( $\text{mg m}^{-3}$ ) with the C2P	RMSE in Chl- <i>a</i> ( $\text{mg m}^{-3}$ ) with the SCI algorithm
From the spring	7.82	0.86
From the summer	6.44	2.87

algorithm was used. The differences between the *in situ* Chl-*a* versus the MERIS-SCI Chl-*a* can be attributed to the high variability in the sediment loads and phytoplankton dynamics in the Changjiang Estuary; this causes bias between *in situ* and satellite samplings. The MERIS-C2P Chl-*a* was mostly overestimated, especially in the case of low Chl-*a* combined with high SSC, which may be an exceptional application of the C2P algorithm.

## 4. Discussion

### 4.1 Chl-*a* variability

The Changjiang Estuary is a very productive and resource-rich aquatic ecosystem (Ning *et al.* 2004). However, because of the limitation of sunlight penetrating the highly turbid sediment-laden waters, the Chl-*a* values are generally lower than 5  $\text{mg m}^{-3}$  in the mouth. The Chl-*a* concentration will increase rapidly when the SSC decreases offshore of the mouth. In addition, low temperatures during the early spring in this area are also a limiting factor for Chl-*a* increase. Seasonal considerations are important when analysing the relationships between nutrient inputs from the Changjiang River and the response of the coastal phytoplankton communities (Zhou *et al.* 2008). The *in situ* Chl-*a* values from the spring cruise were an order of

magnitude lower than those from the summer cruise. The high *in situ* Chl-*a* levels were spatially distributed in the region between the turbidity front and the riverine plume front; these high levels correspond with the moving fronts. In the dry season (e.g. from January to April), the fronts move riverwards from the decrease in river discharges; in the wet season (e.g. from June to October), the fronts move seawards from increased discharges (Chen *et al.* 1988).

#### 4.2 SCI algorithm

The proposed SCI is a compound index of two indicators,  $H_{\text{chl}}$  and  $H_{\Delta}$ .  $H_{\text{chl}}$  has a stronger linear regression with Chl-*a* than  $H_{\Delta}$  does. It can be negative if  $R_{\text{rs}}$  at 665 nm is above the baseline. This indicates that Chl-*a* may be low, such that the  $R_{\text{rs}}$  spectrum is not characterized by chlorophyll pigments; alternatively, the SSC may be so high that the  $R_{\text{rs}}$  spectrum is affected more strongly by the presence of sediment. High scattering from sediment could impair or mask the absorption dip in the  $R_{\text{rs}}$  spectrum.

In addition to the increase in the SSC in turbid sediment-laden waters, the  $R_{\text{rs}}$  amplitude can be enhanced in the whole spectral range. The increase in  $R_{\text{rs}}$  is better detected within the spectral range where absorption is at its minimum (Morel and Bélanger 2006). Morel and Bélanger (2006) proposed that the green part of the spectrum (around 560 nm), *a priori*, is the best candidate for detection of the enhancement; however, in this case,  $R_{\text{rs}}$  at MERIS band 620 nm is more sensitive to the variation in moderate SSC values ranging from 20 to 80 mg l<sup>-1</sup> (Shen *et al.* in press). Thus, it is a promising candidate for detecting SSC variations.  $H_{\Delta}$  has a negative logarithmic relationship with Chl-*a*, and it can be negative if  $R_{\text{rs}}$  at 620 nm is below the baseline, i.e. the opposite to  $H_{\text{chl}}$ . This indicates that the Chl-*a* level is high, and the effect of sediment on  $R_{\text{rs}}$  is smaller. Once the SSC increases, the  $R_{\text{rs}}$  at 620 nm would surpass the baseline and  $H_{\Delta}$  would be positive.

Four MERIS bands were included in the calculations of  $H_{\text{chl}}$  and  $H_{\Delta}$ .  $H_{\text{chl}}$  (employed wavebands: 665, 620 and 681 nm) and  $H_{\Delta}$  (employed wavebands: 620, 560 and 681 nm) versus Chl-*a* have the best fitting regressive functions compared with other MERIS bands. The fit may be improved by more elaborate satellite channels for use in this algorithm.

FLH as an index of Chl-*a* can be applied to satellite estimation of Chl-*a* (Gower *et al.* 1999, Gower and Borstad 2004). Because it seems that FLH (employed wavebands: 665, 681 and 709 nm) has a poor-fit relationship with Chl-*a* in this case (i.e. no function of FLH versus the Chl-*a* has been found for this case), the SCI could instead be a potential proxy of Chl-*a* for turbid sediment-laden waters.

The SCI was designed to be able to extract the Chl-*a* spectral features and not the sediment influences, so that it would be sensitive to Chl-*a* variation. A quadratic polynomial function best fitting the relationship of the SCI versus Chl-*a* was performed on the MERIS image, with the water-leaving radiance reflectance generated by the C2P. Because of the large difference in the Chl-*a* ranges that resulted from the seasonal shifts, regressions of the SCI versus Chl-*a* were applied to the two corresponding MERIS images from the 25 April and 5 August 2008. As a result, the overestimation of Chl-*a* for the turbid sediment-laden waters was corrected. The MERIS-SCI Chl-*a* distribution had a stronger fit with the *in situ* observations, as seen by comparing figures 6 and 2. In conclusion, the SCI algorithm can improve the Chl-*a* estimate for moderate or high SSC in turbid waters.

Although the SCI algorithm for use in the MERIS estimation of Chl-*a* is promising for turbid sediment-laden waters, it has its limitations; the algorithm is primarily dependent on *in situ* data. For the evaluation and validation of the algorithm, a large number of match-ups between concurrent *in situ* and satellite data would be useful. However, it is difficult to obtain large numbers of such match-ups for the Changjiang Estuary and coast because of the frequent cloud coverage over the area. Moreover, the high variability in the SSC and Chl-*a* distributions in the estuary and on the coast prevent the results of the *in situ* samplings from agreeing with those from instantaneous satellite samplings. In addition, the accuracy of MERIS-SCI Chl-*a* is strongly influenced by atmospheric correction. However, atmospheric correction for highly turbid waters is problematic (Doxaran *et al.* 2009). This should be addressed in future work.

## 5. Conclusion

In this paper, we have developed a new indicator for Chl-*a* estimation of turbid sediment-laden waters. The aim was to enhance the derivation of Chl-*a* in the presence of moderate or high concentrations of suspended sediment. A new indicator, the SCI, improved the Chl-*a* estimation of turbid waters, compared with the well-established FLH. The SCI was then related to the actual concentration of Chl-*a* via regression analysis. The results showed that the relationship between the SCI and the Chl-*a* was quadratic, i.e. not linear. The method was able to derive reliable values of Chl-*a* for waters in the estuary, with SSC above 100 mg l<sup>-1</sup>. The proposed method derived spatially realistic patterns of Chl-*a* distribution from MERIS images, which were a close fit with *in situ* observations.

## Acknowledgements

This study was supported by the National Natural Science Foundation of China (no. 40871165). The field campaigns were supported by the Creative Research Groups of China from the NSFC (no. 40721004) and the SKLEC grants (2008KYYW04, 2008KYYW07). The authors are grateful to the young scientists and graduate students of SKLEC for assistance with the *in situ* measurements and sampling during the two surveys. Thanks to the European Space Agency (ESA) for providing MERIS data via the support of the ESA approved Cat-1 project (id 4359). We are grateful to two anonymous reviewers for their helpful comments and suggestions.

## References

- CANNIZZARO, J.P. and CARDER, K.L., 2006, Estimating chlorophyll *a* concentrations from remote-sensing reflectance in optically shallow waters. *Remote Sensing of Environment*, **101**, pp. 13–24.
- CARDER, K.L., REINERSMAN, P.H., CHEN, R.F. and MULLER-KARGER, F., 1993, AVIRIS calibration and application in coastal oceanic environments. *Remote Sensing of Environment*, **44**, pp. 205–216.
- CHEN, J.Y., SHEN, H.T. and YUN, C.X., 1988, *Dynamic Processes and Morphological Evolution of Yangtze Estuary* (Shanghai, China: Shanghai Science and Technology Press) [in Chinese, with English summary].
- DALL'OLMO, G. and GITELSON, A.A., 2005, Effect of bio-optical parameter variability on the remote estimation of chlorophyll-*a* concentration in turbid productive waters: experimental results. *Applied Optics*, **44**, pp. 412–422.

- DALL'OLMO, G. and GITELSON, A.A., 2006, Effect of bio-optical parameter variability and uncertainties in reflectance measurements on the remote estimation of chlorophyll-*a* concentration in turbid productive waters: modeling results. *Applied Optics*, **45**, pp. 3577–3592.
- DASGUPTA, S., SINGH, R.P. and KAFATOS, M., 2009, Comparison of global chlorophyll concentrations using MODIS data. *Advances in Space Research*, **43**, pp. 1090–1100.
- DOERFFER, R. and SCHILLER, H., 2007, The MERIS case 2 water algorithm. *International Journal of Remote Sensing*, **28**, pp. 517–535.
- DOERFFER, R. and SCHILLER, H., 2008, *MERIS Regional Coastal and Lake Case 2 Water Project – Atmospheric Correction ATBD*. GKSS Research Center 21502 Geesthacht Version 1.0, 18 May 2008.
- DOXARAN, D., FROIDEFOND, J.M., CASTAING, P. and BABIN, M., 2009, Dynamics of the turbidity maximum zone in a macrotidal estuary (the Gironde, France): observations from field and MODIS satellite data. *Estuarine, Coastal and Shelf Science*, **81**, pp. 321–332.
- GAO, X. and SONG J., 2005, Phytoplankton distributions and their relationship with the environment in the Changjiang Estuary, China. *Marine Pollution Bulletin*, **50**, pp. 327–335.
- GITELSON, A.A., SCHALLES, J.F. and HLADIK, C.M., 2007, Remote chlorophyll-*a* retrieval in turbid, productive estuaries: Chesapeake Bay case study. *Remote Sensing of Environment*, **109**, pp. 464–472.
- GITELSON, A.A., DALL'OLMO, G., MOSES, W., RUNDQUIST, D.C., BARROW, T., FISHER, T.R., GURLIN, D. and HOLZ, J., 2008, A simple semi-analytical model for remote estimation of chlorophyll-*a* in turbid waters: validation. *Remote Sensing of Environment*, **112**, pp. 3582–3593.
- GONS, H.J., AUER, M.T. and EFFLER, S.W., 2008, MERIS satellite chlorophyll mapping of oligotrophic and eutrophic waters in the Laurentian Great Lakes. *Remote Sensing of Environment*, **112**, pp. 4098–4106.
- GOWER, J.F.R. and BORSTAD, G.A., 2004, On the potential of MODIS and MERIS for imaging chlorophyll fluorescence from space. *International Journal of Remote Sensing*, **25**, 1459–1464.
- GOWER, J.F.R., DOERFFER, R. and BORSTAD, G.A., 1999, Interpretation of the 685 nm peak in water leaving radiance in terms of fluorescence, absorption and scattering, and its observation by MERIS. *International Journal of Remote Sensing*, **20**, pp. 1771–1786.
- HE, Q., YUN, C.X. and SHI, F.R., 1999, Remote sensing analysis for suspended sediment concentration in water surface layer in Yangtze River estuary. *Progress in Natural Science*, **9**, pp. 160–164 (in Chinese, with English abstract).
- INTERNATIONAL OCEAN-COLOUR COORDINATING GROUP (IOCCG), 2000, *Remote Sensing of Ocean Color in Coastal, and Other Optically-Complex, Waters*, S. Sathyendranath (Ed.). Reports of the IOCCG Group, No. 3, Dartmouth, Canada.
- INTERNATIONAL OCEAN-COLOUR COORDINATING GROUP (IOCCG), 2006, *Remote Sensing of Inherent Optical Properties: Fundamentals, Tests of Algorithms, and Applications*, Z.-P. Lee (Ed.). Reports of the IOCCG, No. 5, Dartmouth, Canada.
- JOINT GLOBAL OCEAN FLUX STUDY (JGOFS), 1998, Standard Protocol for Measurement of Chlorophyll. Available online at: <http://ocean.stanford.edu/cal/>.
- KOMICK, N.M., COSTA, M.P.F. and GOWER, J., 2009, Bio-optical algorithm evaluation for MODIS for western Canada coastal waters: an exploratory approach using in situ reflectance. *Remote Sensing of Environment*, **113**, pp. 794–804.
- KONG, Y.Z., DING, P.X., HE, S.L., HE, C. and XIAO, W.J., 2006, Analysis of spatial and temporal variation characteristics of suspended sediment concentration in the Changjiang River Estuary and adjacent sea area. *Advances in Marine Science*, **24**, pp. 446–454 (in Chinese with English abstract).

- LEE, Z.P., CARDER, K.L., PEACOCK, T.G., DAVIS, C.O. and MUELLER, J.L., 1996, Method to derive ocean absorption coefficients from remote-sensing reflectance. *Applied Optics*, **35**, pp. 453–462.
- LI, J.F., SHI, W.R. and SHEN, H.T., 1994, Sediment properties and transportation in the turbidity maximum in Changjiang estuary. *Geographical Research*, **13**, pp. 51–59 (in Chinese with English abstract).
- MOBLEY, C.D., 1999, Estimation of the remote-sensing reflectance from above-surface measurements. *Applied Optics*, **38**, pp. 7442–7455.
- MOREL, A. and BÉLANGER, S., 2006, Improved detection of turbid waters from ocean color sensors information. *Remote Sensing of Environment*, **102**, pp. 237–249.
- NATIONAL AERONAUTICS AND SPACE ADMINISTRATION (NASA), 2003, *Ocean Optics Protocols for Satellite Ocean Color Sensor Validation*, Revision 4, Volume: Radiometric Measurements and Data Analysis Methods, NASA/TM-2003-211621/Rev4-Vol.III.
- NING, X.R., SHI, J.X., CAI, Y.M. and LIU, C.G., 2004, Biological productivity front in the Changjiang Estuary and the Hangzhou Bay and its ecological effects. *Acta Oceanologica Sinica*, **26**, pp. 96–106 (in Chinese with English abstract).
- O'REILLY, J.E., MARITORENA, S., MITCHELL, B.G., SIEGEL, D.A., CARDER, K.L., GARVER, S.A., KAHRU, M. and MCCLAIN, C., 1998, Ocean colour chlorophyll algorithms for SeaWiFS. *Journal of Geophysical Research*, **103**, pp. 24 937–24 953.
- SALAMA, M.S., DEKKER, A., SU, Z., MANNAERTS, C. and VERHOEF, W., 2009, Deriving inherent optical properties and associated inversion-uncertainties in the Dutch Lakes. *Hydrology and Earth System Sciences*, **13**, pp. 1113–1121.
- SHEN, Z.L., 1991, A study of the effects of the three gorge project on the distributions and changes of the nutrients in the Changjiang River estuary. *Oceanologia et Limnologia Sinica*, **22**, pp. 540–546 (in Chinese with English abstract).
- SHEN, Z.L., 2004, Nitrogen transport fluxes in the Yangtze River. *Advances in Water Science*, **15**, pp. 752–759 (in Chinese with English abstract).
- SHEN, F., VERHOEF, W., ZHOU, Y.X., SALAMA, MHD.S. and LIU, X.L., In press, Satellite estimates of wide-range suspended sediment concentrations in Changjiang (Yangtze) estuary using MERIS data. *Estuaries and Coasts*, doi: 10.1007/s12237-010-9313-2.
- TREES, C.C., BIDIGARE, R.R., KARL, D.M., VAN HEUKELEM, L. and DORE, J., 2003, *Ocean Optics Protocols for Satellite Ocean Colour Sensor Validation*, Revision 5, Volume V: Biogeochemical and Bio-Optical Measurements and Data Analysis Protocols, chapter 3 NASA /TM-2003, pp. 15–24.
- WOŹNIAK, S.B. and STRAMSKI, D., 2004, Modeling the optical properties of mineral particles suspended in seawater and their influence on ocean reflectance and chlorophyll estimation from remote sensing algorithms. *Applied Optics*, **43**, pp. 3489–3503.
- ZHOU, M.J., SHEN, Z.L and YU, R.C, 2008, Responses of a coastal phytoplankton community to increased nutrient input from the Changjiang (Yangtze) River. *Continental Shelf Research*, **28**, pp. 1483–1489.
- ZHU, J.R., 2004, The concentration distribution of chlorophyll-*a* of sea on Changjiang port and its causation analysis. *Science in China Series D*, **34**, pp. 757–762.